

## **Crippling of Thin-Walled Composite Sections using Progressive Failure Analysis**

Scott Malaznik

Senior Staff Engineer

Lockheed Martin Aeronautics Company, Palmdale, California 93599

### **Summary**

Aircraft structures, both metallic and composite, are often stiffened with thin-walled sections of various shapes to resist compression loads efficiently. Analysis of these structures can be challenging, and empirical methods are often used for design purposes. Since initial buckling is not necessarily indicative of structural failure, the analysis must be carried into the post-buckling range, where geometric and material nonlinearities are present. Final failure in this context is called crippling, which corresponds to the maximum load carried by the section.

In this paper, the nonlinear capabilities of MSC Nastran SOL 400 are used to perform post-buckling analysis of graphite/epoxy composite I-section stiffeners. After performing an eigenvalue buckling analysis, initial imperfections in the shape of the buckling modes are applied to the model to start the large displacement analysis. Composite material failures are modeled using the Progressive Failure Analysis (PFA) feature of SOL 400. Results are plotted as load-displacement curves, and crippling failure is defined as the maximum load carried. Results are compared to published test data as well as MIL-HDBK-17 design equations.

### **Introduction**

Thin-walled sections, composed of either metallic or composite materials, are commonly used in the design of aircraft structures. Thin sections are prone to buckling, rather than material, failures under compression loads, and therefore buckling analysis is of major importance in the structural design of aircraft. It is well known that the initial buckling of thin walled structures does not necessarily result in immediate failure, and this inherent post-buckling capability can be used to achieve light weight designs. Indeed, recognition of the post-buckling load carrying capability of metal structures helped make possible the transition from wood to metal aircraft structures that occurred in the 1930s.

The buckling behavior of a thin-walled column is a function of its length (see Fig. 1). A long column will buckle in long waves (on the order of its length) with the cross-sections translating, and perhaps rotating, but maintaining their shape. Long column, or global, buckling is represented by the classical Euler formula, and such columns do not exhibit significant post-buckling capability. For a short column, the initial buckling mode consists of short waves (on the order of the component plate widths) with the corners of the cross-section remaining straight. This type of buckling is called local buckling and depending on their geometry, such sections may exhibit significant post-buckling capability. The Johnson-Euler curve is an empirical relation often used in the intermediate column range.

An abbreviated description of the post-buckling behavior of thin plates is given here to provide background for this study. Detailed discussions can be found in many sources (for example, see Ref. 1). When a thin flat rectangular plate supported on all edges buckles under axial compression, the plate bends out of its initial plane. If the plate is visualized as a collection of strips parallel to the load direction, it can be seen that after buckling the strips near the edges remain nearly flat, while the curvature of the strips increases towards the middle. The axial stiffness of these strips is a function of their curvature, with flatter strips being stiffer and more curved strips being less stiff. Therefore, the stiffness distribution varies across the width of the plate. This gives rise to the characteristic cosine distribution of stresses across the plate width.

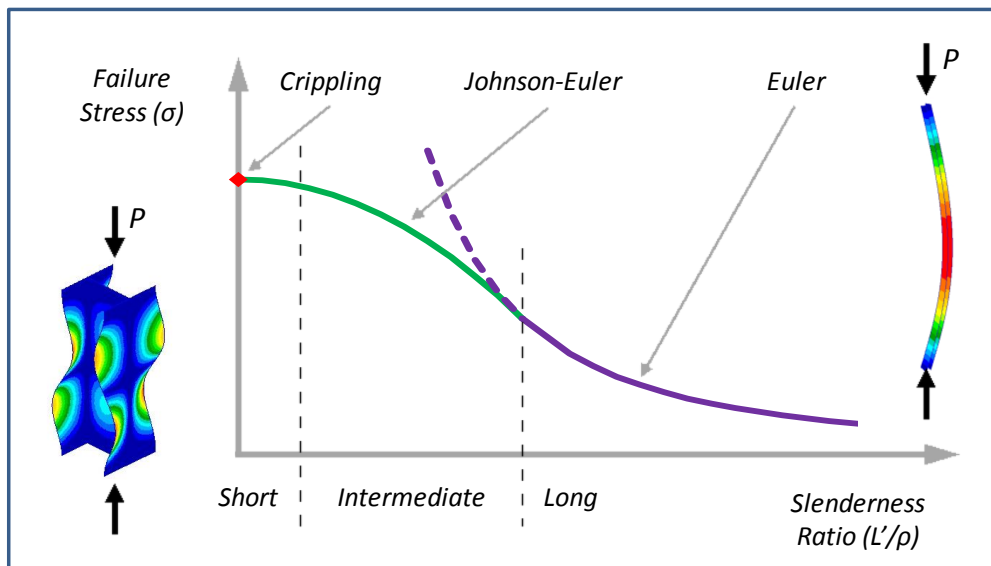


**Fig. 1 Column buckling behavior as a function of length**

The total stiffness of the post-buckled plate is less than that of the initially flat plate, as shown in a load-displacement diagram (Fig. 2). Although the plate has buckled and its stiffness has decreased, perhaps by about half, it can still carry increasing loads. Up to this point, the material may still be linear elastic, in which case, the nonlinearities are caused by large displacements only. At some point however, material degradation begins and the plate stiffness decreases rapidly leading to failure. This “degradation” is due to plasticity in metallic materials, and local ply failures and/or delaminations in laminated composite materials.

The pre- and post-buckling paths are both valid equilibrium states, so in a numerical analysis, an initially flat plate may follow the pre-buckling path even beyond the buckling load. To ensure the plate shifts to the secondary post-buckling curve, an external agent is often introduced into the analysis. One common approach is to deform the initially flat geometry out-of-plane by a small amount before applying the load. The shape of this “initial imperfection” is often taken in the form of a buckling mode, with the amplitude of the mode being set to a relatively small

value, perhaps 0.1 to 0.5 times the plate thickness. This geometric imperfection can be viewed as representing unavoidable small deviations from flatness of a real plate.

Due to the geometric and material nonlinearities involved in crippling failures, empirical methods are usually used in the design of aircraft structures. Methodology for crippling of metals was developed in the 1930s and is well documented in NACA-TN-3784 (Ref. 2). An analogous approach for composites was developed in the 1970s and is documented in MIL-HDBK-17 (Ref. 3). Refer to these documents for details on the available empirical crippling prediction methodologies.

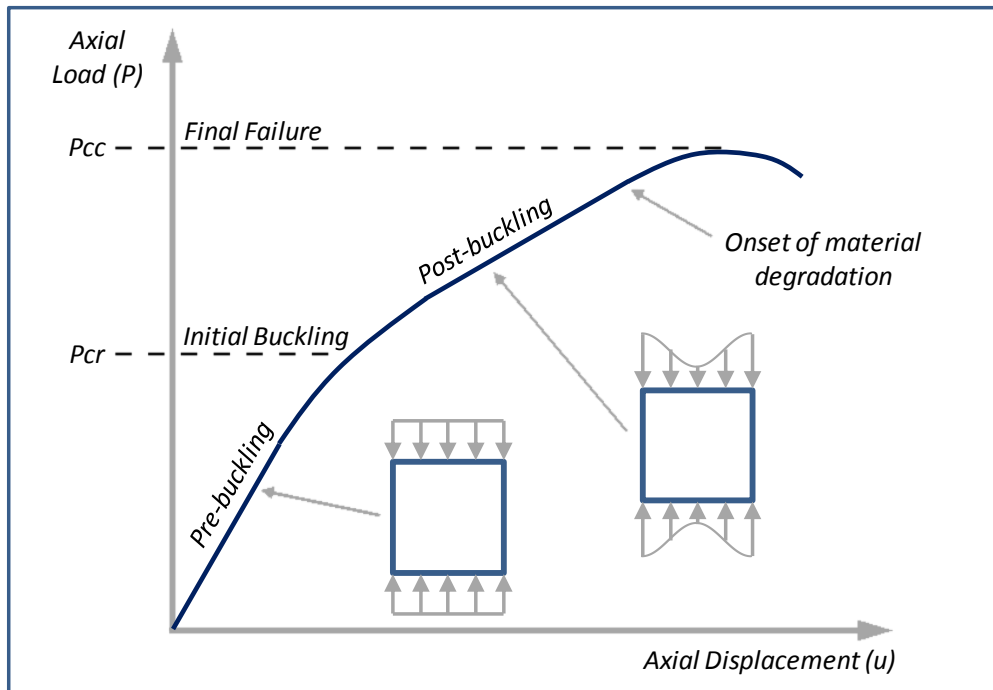


**Fig. 2 Typical load-displacement behavior of a thin plate**

### **Approach**

The purpose of this study was to assess the applicability of the Progressive Failure Analysis feature of MSC Nastran SOL 400 to crippling analysis of thin-walled composite sections. For expediency, the geometry and material used in this study were selected to match those of Ref. 4, so that the analysis results could be compared to the test data of that paper. Although Ref. 4 considered various cross sections, only one was considered here: an I-section with the dimensions shown in Fig. 3a. As typical for crippling tests, the member lengths were short enough to avoid column buckling and ensure local buckling modes were critical. Also, the flange width is large relative to the web height so that local buckling of the flange is expected to occur first. Four different lengths were analyzed (4, 6, 8, and 12 inches) but test data was only available in Ref. 4 for two of the lengths (4 and 8 inches).

The four finite element models were constructed entirely from 0.125" square CQUAD4 elements, giving 10 elements across the web and 6 elements across each flange, with the number of elements along the length proportional to the member length. The 4 inch model had a total of 1088 elements and the 12 inch model had 3264 elements (see Fig. 4). This level of detail was deemed sufficient to capture the local buckling modes as well as being consistent with the goal of making a quick preliminary assessment of the Progressive Failure Analysis capability.

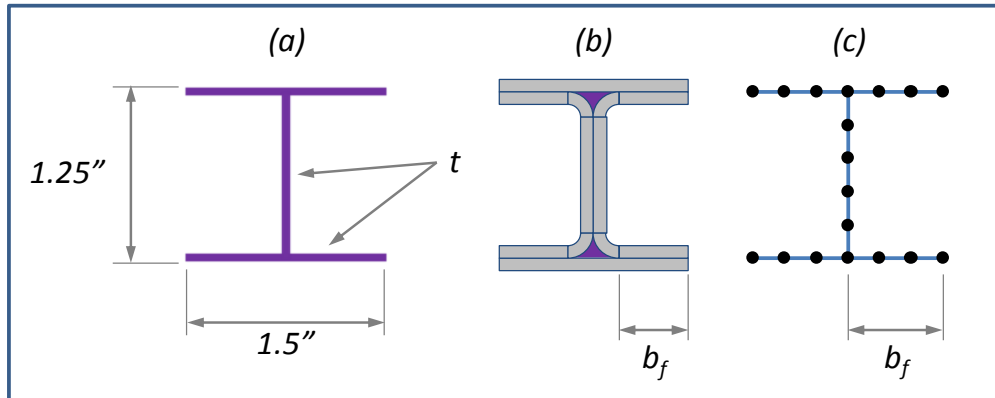


**Fig. 3 Member cross-section. (a) Dimensions, (b) Test specimen laminate detail (thickness exaggerated), (c) Finite element discretization (not all nodes shown)**

No attempt was made to represent the details of the web to flange intersection. In the test specimens, the web laminate splits into two halves which bend outwards to form half of the flange thickness, as shown in Fig. 3b. In Ref. 4, the intersection radius was varied and found to have a large effect on the results, probably because it affects the width of the outstanding flange as well as affecting the amount of unidirectional filler material present. The finite element model does not represent these corner details (Fig. 3c). This omission was considered acceptable for performing a quick assessment of the SOL 400 PFA capability, with the understanding that future work may be required to fully capture such additional features in the model.

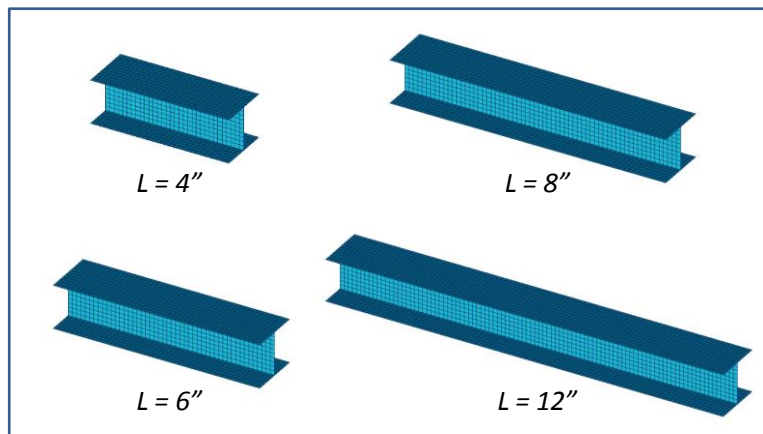


**Fig. 4 Finite Element Models**

Following Ref. 4, the material used was graphite/epoxy AS4/3502 unidirectional tape with the properties listed in Table 1. The ply material properties were defined in Nastran using a MAT8 card, and the laminate layups were defined using a PCOMP card. The ply material strength values for use in the maximum stress failure criterion are listed in Table 2 and were defined using a MATF card, which is unique to the SOL 400 PFA capability. Three balanced and symmetric laminate layups were used: an 8 ply quasi-isotropic (designated L8), a 16 ply quasi-isotropic (L16A), and a 16 ply orthotropic (L16B), which are listed along with their effective elastic constants in Table 3. The 16 ply “orthotropic” laminate has more zero degree plies than the corresponding quasi laminate.

**Table 1. AS4/3502 Graphite/Epoxy Unidirectional Tape Elastic Constants**

E1 psi	E2 psi	nu12	G12 psi	G1Z psi	G2Z psi	tply in
1.85E+07	1.64E+06	0.30	8.70E+05	8.70E+05	5.80E+05	0.005

**Table 2. AS4/3502 Graphite/Epoxy Strength Values**

S11T psi	S11C psi	S22T psi	S22C psi	S33T psi	S33C psi	S12 psi	S23 psi	S31 psi
210000	210000	7540	29900	7540	29900	13500	13500	13500

**Table 3. Laminate Layup Definitions and Effective Elastic Constants**

ID	Layup	Ex psi	Ey psi	nuxy	Gxy psi	tlam in
L8	[45/-45/0/90] <sub>s</sub>	7.42E+06	7.42E+06	0.30	2.85E+06	0.040
L16A	[45/-45/0/90] <sub>2s</sub>	7.42E+06	7.42E+06	0.30	2.85E+06	0.080
L16B	[45/-45/-45/45/90/0] <sub>3s</sub>	9.28E+06	5.45E+06	0.41	2.85E+06	0.080

As typical for crippling tests, the ends of the test specimens were embedded in a 1 inch deep cylinder of solid aluminum-epoxy potting compound enclosed in a circular aluminum ring. This ensures uniform introduction of the compression load, and helps prevent brooming failures of the ends. The axial displacements and all rotations were restrained at each end of the models (Fig. 5). The ends were left free to expand laterally, as it was desired to avoid local stress concentrations there. Enforced axial displacements are applied at one end, and the resulting reaction force at the other end corresponds to the applied load.

A linear eigenvalue analysis using Nastran SOL 105 was performed to compute the initial buckling loads and mode shapes of each model. The first 5 modes were obtained, and each mode shape was visually inspected in MSC Patran to ensure that valid local buckling modes

occurred. The magnitude and location of the maximum out-of-plane flange displacement was noted for later use in defining the initial geometric imperfections, as discussed next.

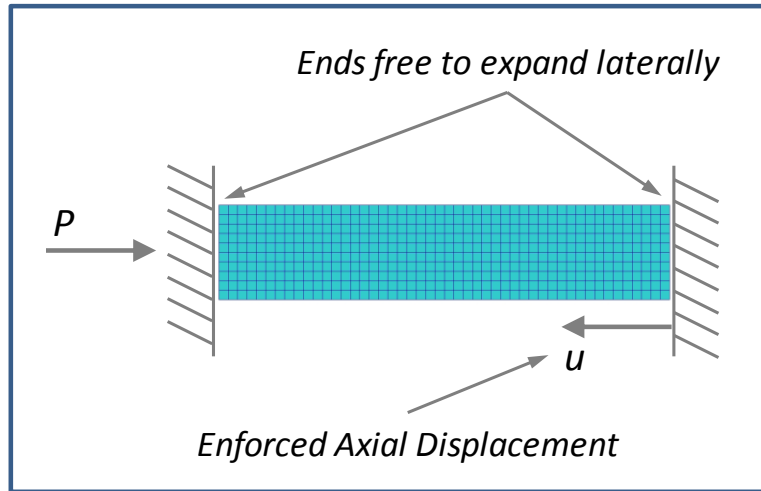


**Fig. 5 Finite Element Model Boundary Conditions**

To ensure that the cross section web and flange plates follow the post-buckling path rather than remain flat, the initial geometry of the mesh was slightly deformed. The shape of the imperfection was defined using a selected buckling mode shape, which was scaled so that the maximum deformation was equal to a desired small value (see Fig. 6). For most of the analyses, the first buckling mode was used as the imperfection shape and the amplitude was set to 0.02 inches, which was one-half of the thickness of the 8 ply laminate. For comparison, several runs were made using other imperfection magnitudes and a few were made using the second buckling mode as the imperfection shape. The Patran "Results/Results/Combine" utility was used to offset the original nodes to the slightly deformed configuration.

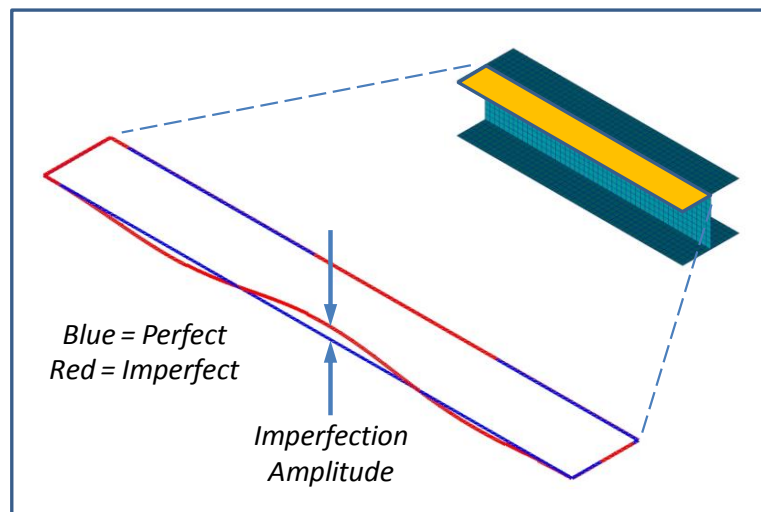


**Fig. 6 Definition of Initial Geometric Imperfection**

Using the slightly deformed geometry as the starting point, nonlinear analysis was performed using Nastran SOL 400, including large displacements and composite material failure using Progressive Failure Analysis. The LGDISP parameter was used to activate large displacements, and a MATF card was used to define the material failure parameters. Default values were used for most of the other nonlinear analysis parameters, such as those controlling load stepping, stiffness updates, and convergence tolerances.

The PFA methodology offers several options for composite material failure criteria, including maximum stress, maximum strain, Hill, Hoffman, Tsai-Wu, Hashin, and Puck (see the Nastran Quick Reference Guide, Ref. 5). Some criteria require parameters which may not be readily available for a given material. The maximum stress criterion was used exclusively in this study, using the ply strength values listed in Table 2 (Ref. 4). This criterion was selected because the required strength parameters were readily available, and not necessarily because it was thought to be the most accurate option.

In the PFA methodology, once initial damage is identified by the selected failure criterion, the ply stiffnesses are degraded according to the type of failure found. The rate of degradation can be selected as immediate or gradual, and all results reported here used the gradual option. The degraded material properties are used to re-compute the element stiffnesses, and the load stepping then continues. The stiffness changes due to local damage cause load re-distribution between different parts of the member. When enough elements have failed locally, the global stiffness of the member starts to decrease. Final failure occurs when the stiffness drops to zero and the member cannot carry additional load.

### Buckling Analysis

The initial buckling loads computed by SOL 105 for the 4 lengths and 3 laminates are listed in Table 4. Every mode shape was examined visually in Patran, and in all cases the initial buckling mode was a local mode, as indicated by the web-flange intersections remaining straight while the webs and flanges buckled. The largest buckles were in the flanges, as expected due to the ratio of flange height to web width defined for the cross-section. The initial buckling modes for the 4 lengths of the 8 ply quasi-isotropic sections are shown in Fig. 7.

**Table 4. Initial Buckling Loads (Test data from Ref.4, with corner radius = 0.125")**

Length (in)	Buckling Loads (lb)					
	Layup L8		Layup L16A		Layup L16B	
	FEA	Test	FEA	Test	FEA	Test
4	2946	5290	20960	26710	22076	30290
6	2774	N/A	19679	N/A	21200	N/A
8	2706	5290	19170	26570	20871	28190
12	2652	N/A	18777	N/A	20625	N/A

The corresponding test buckling loads from Ref. 4 are also listed in Table 4. These test specimens had a corner radius of 0.125". The FEA buckling loads are significantly (22%-49%) lower than the test values. Several points can be made about this difference. First, the finite element models do not represent the web-flange intersection in any detail. As seen in Fig. 3b, the presence of the corner radius means that the effective width of the flange is less than it is in the FEM. Therefore, the flange buckling load should be higher, and a larger radius should correspond to a higher buckling load, which is what the test data shows. Second, the transition from pre- to post-buckling paths is gradual, and it can be difficult to determine precisely the buckling point from a test. Ref. 6 discusses several methods for determining buckling loads from tests, but Ref. 4 does not explain in detail how buckling loads were determined so it is difficult to make a fair comparison. Finally, buckling does not constitute failure for these specimens, so the magnitude of the buckling loads is of less importance than the failure loads, which are the primary concern of this study. Therefore, no additional effort was made to explain these differences.

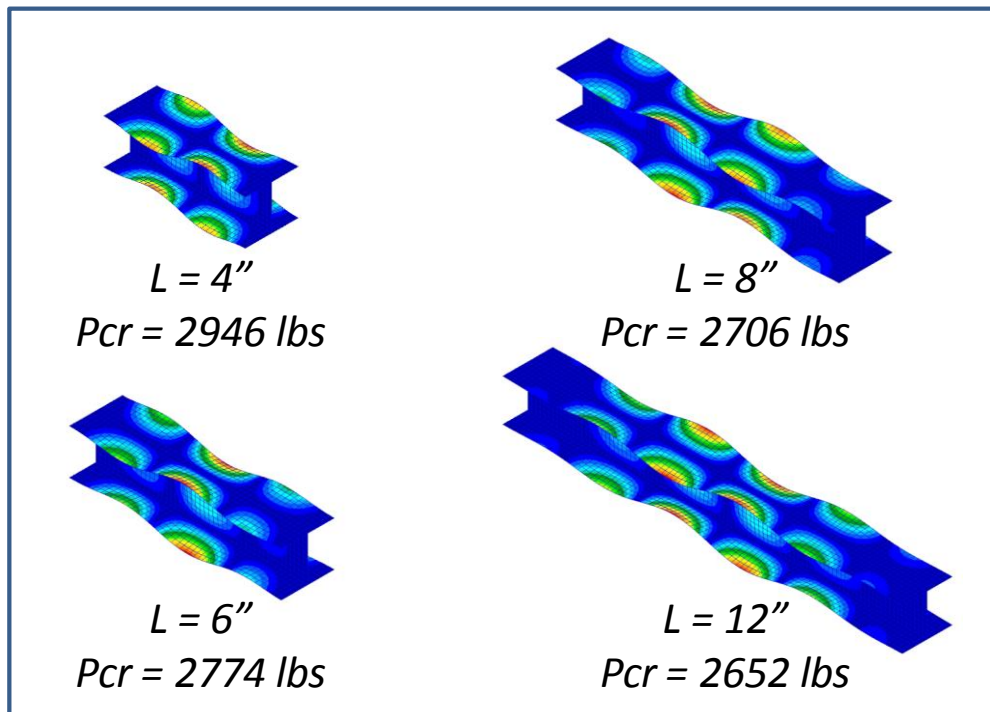


**Fig. 7 Initial buckling modes, 8 ply quasi-isotropic laminate**

### Nonlinear Analysis

A load-displacement diagram was constructed for each nonlinear run. Fig. 8 shows the diagram for the 4 inch specimen with the 8 ply quasi-isotropic laminate. The initial imperfection in this case had the shape of the first buckling mode, with an amplitude of 0.01 inch (corresponding to ¼ the flange thickness). The curve shows the expected characteristics discussed in regards to Fig. 2. The initial slope corresponds to the member axial stiffness given by  $AE/L$ . Near the



buckling load of 2946 lbs, the curve smoothly bends to a secondary linear part with a slope of about  $\frac{1}{2}$  the initial slope. Although not apparent from the diagram, there is no material damage until a load of 6046 lbs is reached, which is about 2 times the buckling load. Although local damage continues to increase with load, it does not noticeably affect the global stiffness until about 7500 lbs. After that, the stiffness decreases rapidly until the maximum load of 8351 lbs is reached, which is 2.8 times the initial buckling load and 1.4 times the initial damage load. Without the PFA capability, the initial damage load of 6046 lbs would probably have been deemed the “failure” load of the part if initial buckling had been allowed.

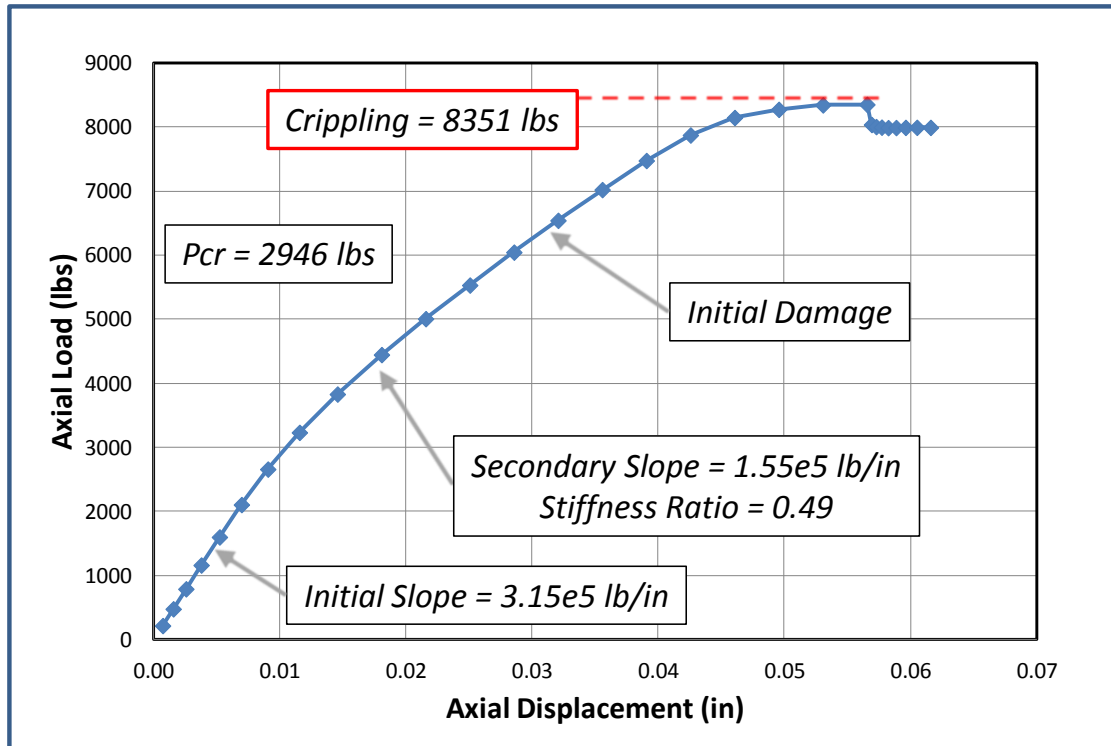


**Fig. 8 Load-displacement curve for 4 inch specimen, 8 ply quasi-isotropic laminate**

The effect of different imperfection magnitudes was also considered. Fig. 9 shows the case of the 4 inch specimen with the 8-ply laminate. Both the first and second buckling modes were considered as the imperfection shape, and the amplitude was varied from 0.004” (1/10 the flange thickness) to 0.04” (equal to the flange thickness). It is seen that increasing imperfection amplitudes tend to smooth out the transition between the pre- and post-buckling slopes. For small values of the imperfection magnitude, the crippling loads did not vary greatly (see inset table in Fig. 9). It is reasonable to expect the occurrence of small imperfections in practice, perhaps on the order of 1/10 the flange thickness, but values near the flange thickness are not very likely. For imperfections up to  $\frac{1}{4}$  the flange thickness, the crippling load varied by less than 1%, whether the imperfection shape was the first or second buckling mode.

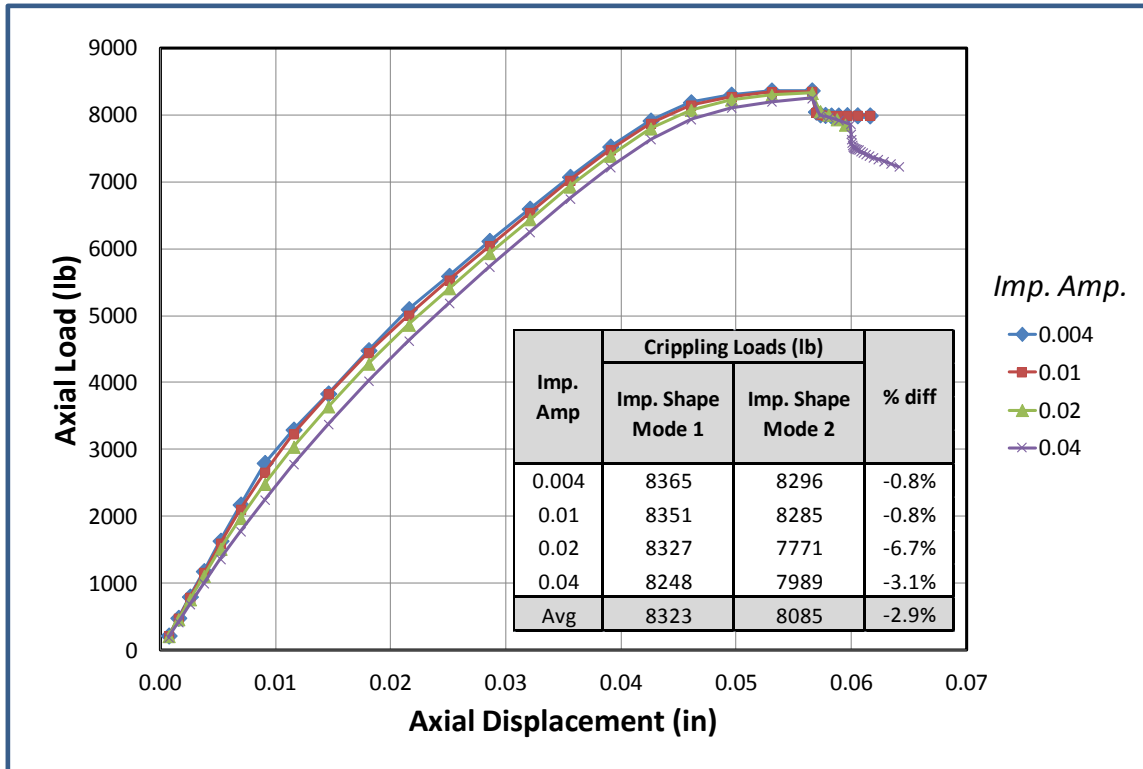


**Fig. 9 Effect of different imperfection magnitudes**

Damage locations and the growth of damage with load are shown in Fig. 10 for the case of the 6 inch member with the 8 ply quasi-isotropic laminate. At the buckling load, there is no material damage anywhere in the member. The first damage occurs at a load level of 5591 lbs (2 times the buckling load). The SOL 400 damage parameter indicates the reduction in stiffness of an element computed by the PFA algorithm. A damage value of 0.0 corresponds to no damage (100% stiffness) while a value of 1.0 corresponds to 100% damage (zero stiffness). In this case, the damage occurs in the outer plies on the crest of the largest buckle wave, where overall axial compression combines with compression due to local bending. Damage occurs at one element initially, but as the load increases, the damage increases in the damaged elements as well as spreading to other elements. Also shown in Fig. 10 is an intermediate load level, as well as at the maximum load of 8018 lbs. Even at the maximum load, no element has reached 100% damage (element stiffness reduced to zero). Rather, it is the spatial extent of the damage that causes the overall stiffness of the member to decrease, resulting in failure.

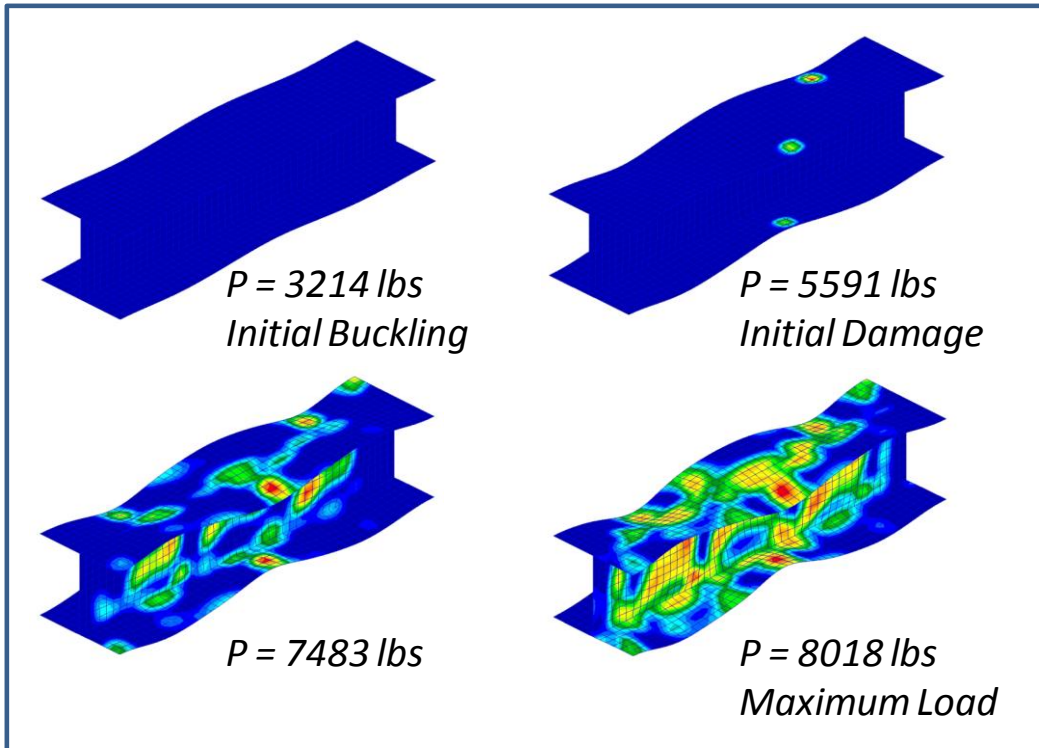


**Fig. 10 Growth of damage with increasing load**

### Comparisons

The crippling loads obtained using SOL 400 are compared to the corresponding test data from Ref. 4 in Figs. 11a-c. The 8 ply quasi-isotropic laminate is shown in Fig. 11a, the 16 ply quasi laminate in Fig. 11b, and the 16 ply orthotropic laminate in Fig. 11c. The SOL 400 predictions range from 12.2% low to 4.5% high compared to the test data, which is considered a good comparison. In 5 out of the 6 cases, the test specimens failed at loads higher than predicted by SOL 400, which is the preferable direction.

The SOL 400 crippling loads are compared to design allowables obtained using the methodology of MIL-HDBK-17 (Ref. 3) in Fig 12a-c. The 8 ply quasi-isotropic laminate is shown in Fig. 12a, the 16 ply quasi laminate in Fig. 12b, and the 16 ply orthotropic laminate in Fig. 12c. The length range shown in these curves (4-12 inches) is in the very short column range, so the MIL-17 allowable curve is very flat. For the 8 ply quasi laminate (Fig. 12a) the SOL 400 results are close to the MIL-17 allowable curve. For the 16 ply laminates (Fig. 12b-c), the MIL-17 curve is about 20-30% lower than the SOL 400 predictions. Since the test data is generally greater than the FEA predictions, the MIL-17 allowables are seen to be conservative with respect to both test and FEA values for these laminates, which is appropriate for a design method. It was not immediately apparent why the 8-ply laminate was close and the 16-ply laminate was reasonably conservative.

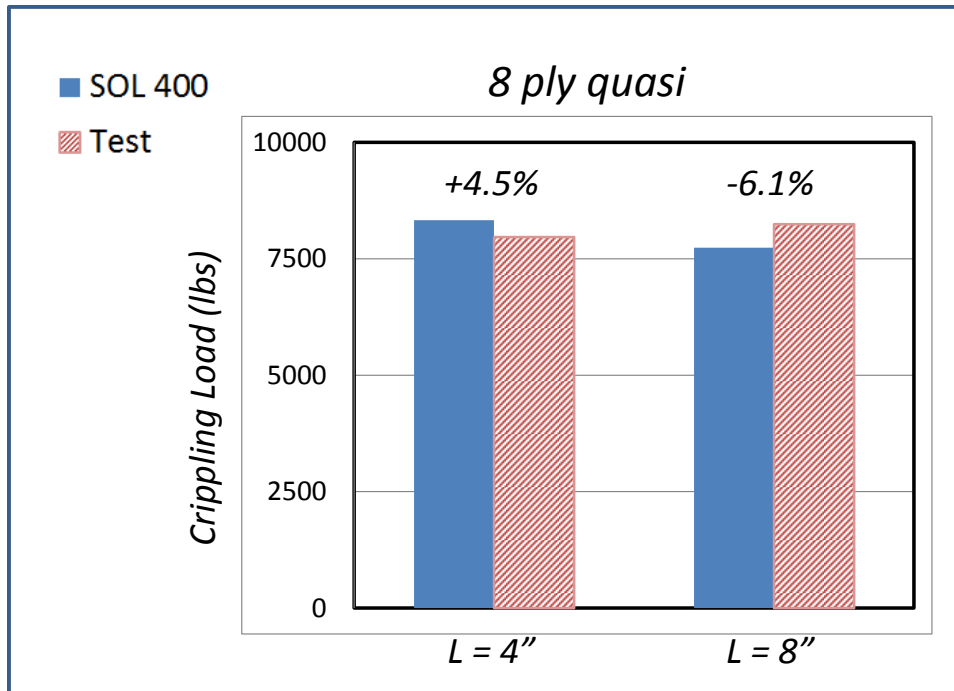


**Fig. 11 (a) Comparison with Test Data (L8 Quasi-Isotropic Layup)**

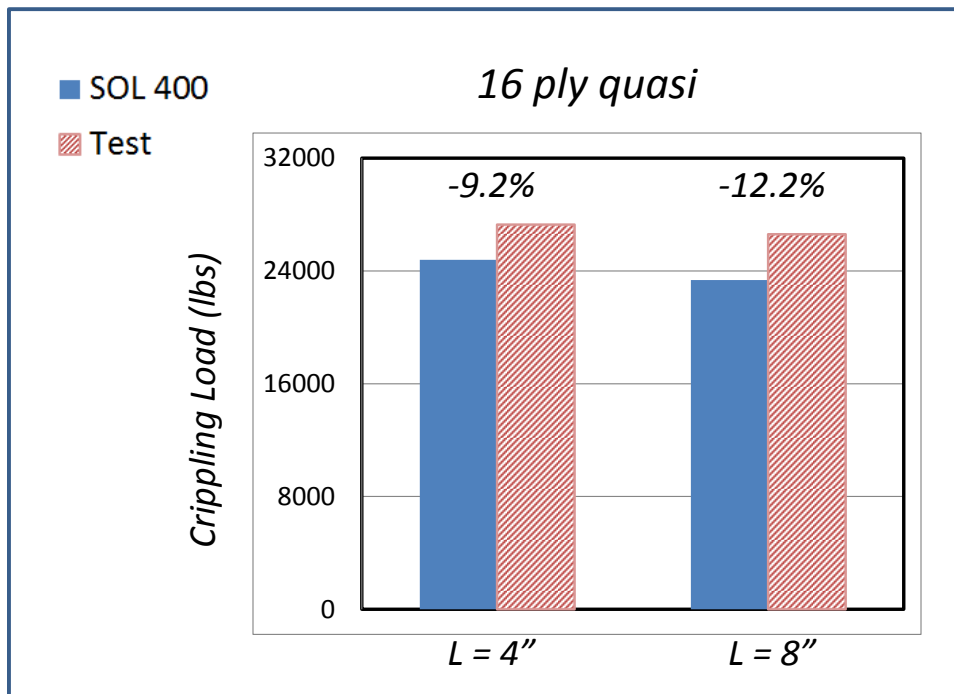


**Fig. 11 (b) Comparison with Test Data (L16A Quasi-Isotropic Layup)**

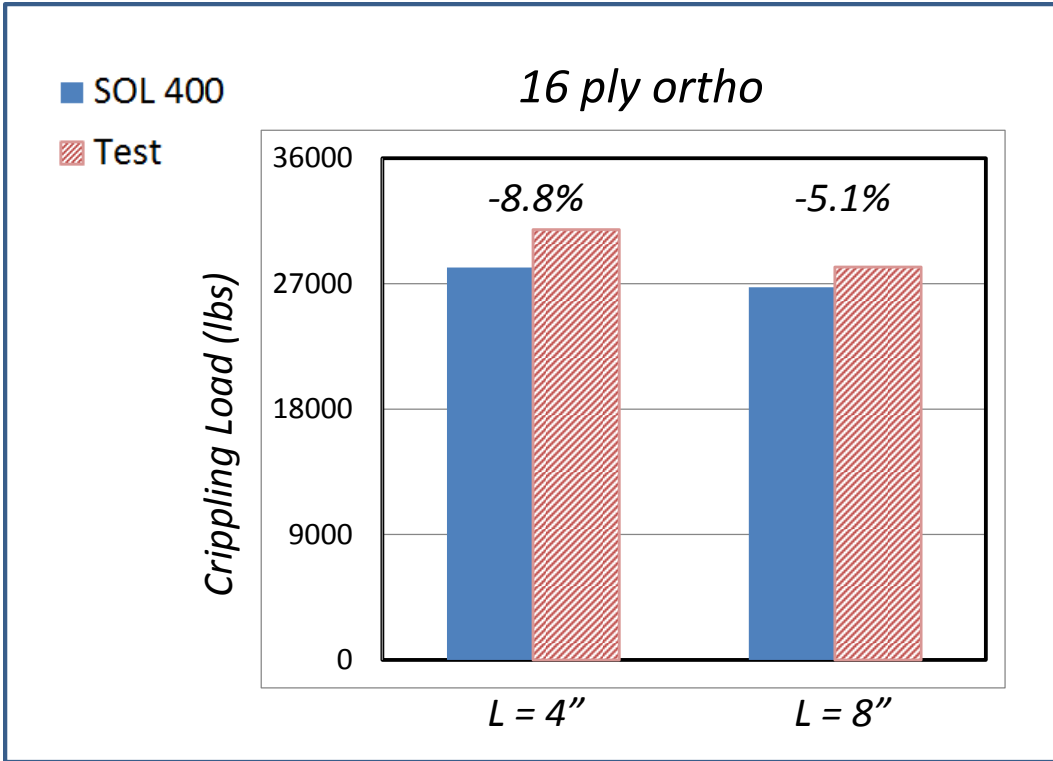


**Fig. 11 (c) Comparison with Test Data (L16B Orthotropic Layup)**

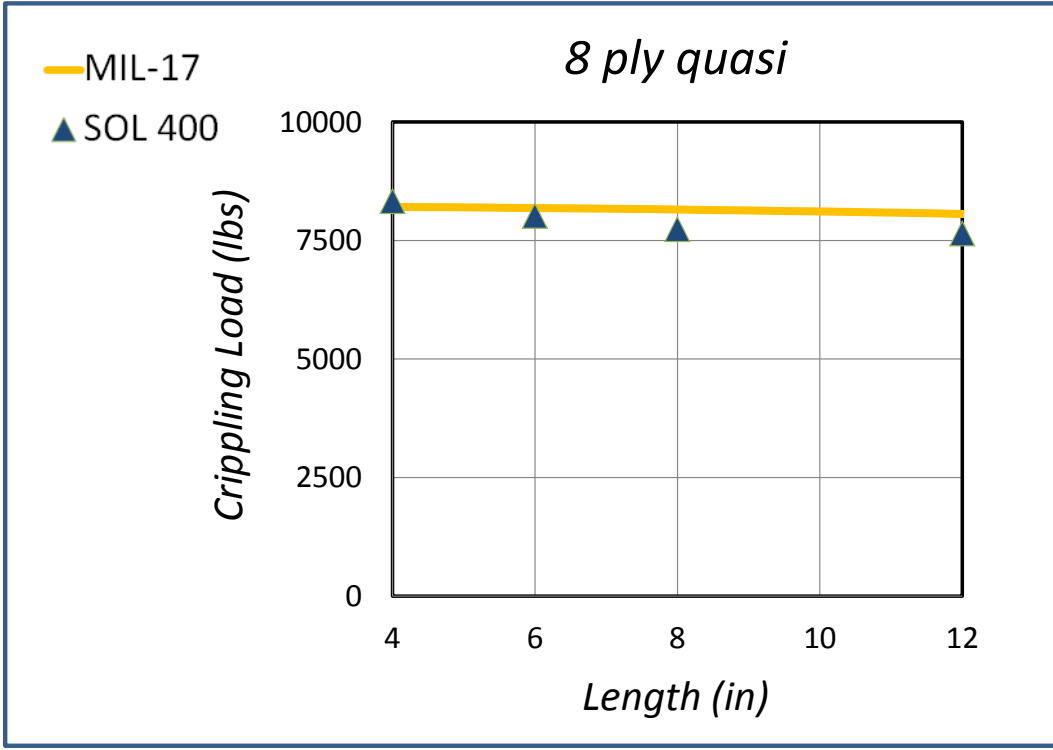


**Fig. 12 (a) Comparison with MIL-HDBK-17 (L8 Quasi-Isotropic Layup)**

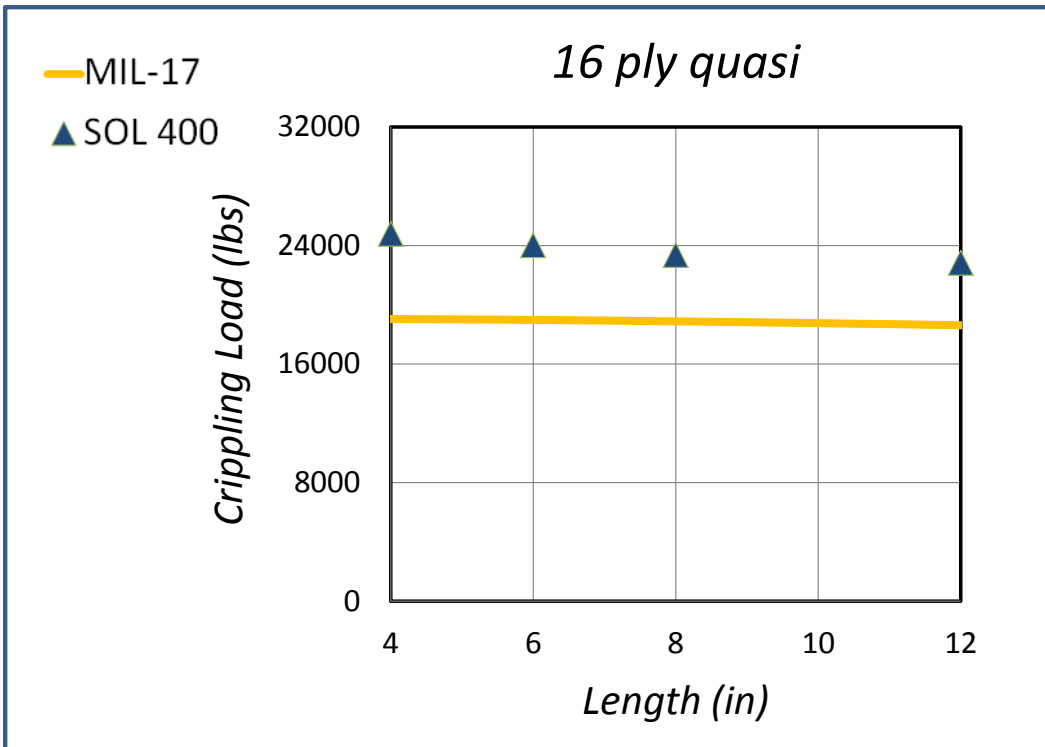


**Fig. 12 (b) Comparison with MIL-HDBK-17 (L16A Quasi-Isotropic Layup)**

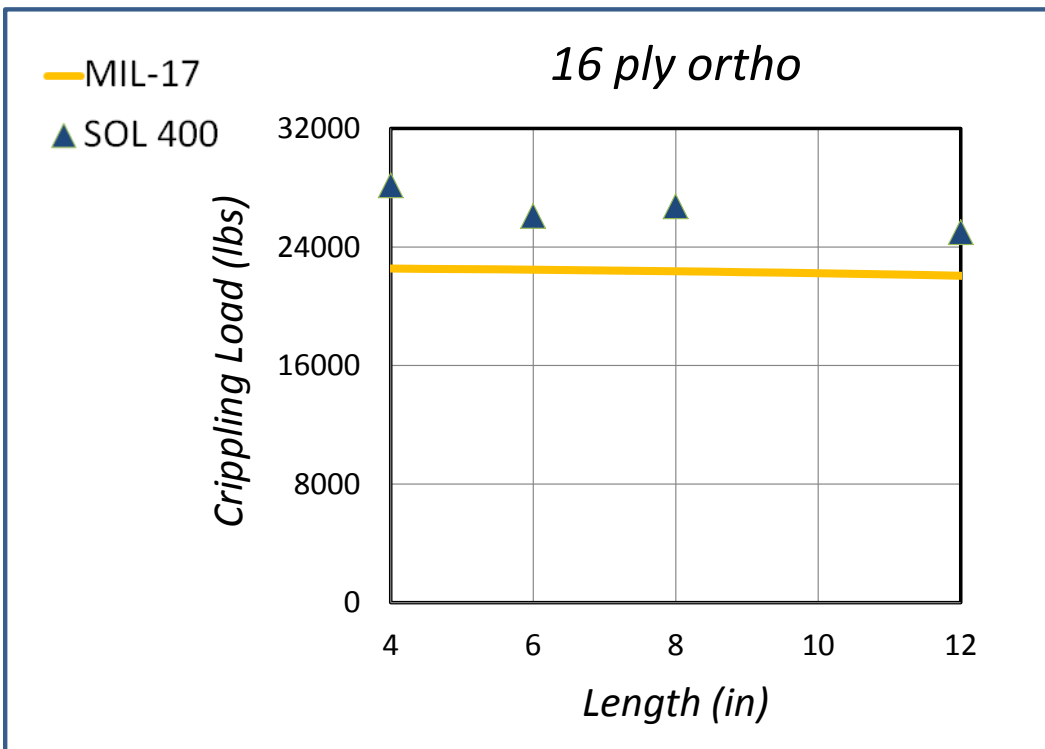


**Fig. 12 (c) Comparison with MIL-HDBK-17 (L16B Orthotropic Layup)**

## Conclusions

The nonlinear load-displacement curves obtained using SOL 400 with PFA followed the expected trends, and the predicted crippling loads agreed fairly well with available test data (+4.5% to -12.2%). The initial buckling loads obtained using SOL 105 were significantly lower than test (-22% to -49%). These differences may be due to deficiencies in the model or difficulties in determining initial buckling from a test and although not pursued here are worth further investigation.

The MIL-HDBK-17 derived crippling allowables are close to FEA predictions for the 8-ply laminates, but are about 20-30% low for the 16-ply laminates. As a design methodology, rather than a prediction tool, it is appropriate that the MIL-17 values are conservative with respect to both test and FEA, but it was not discovered why there was a difference between the 8-ply and 16-ply laminates in this regard.

Here, we only used buckling and crippling loads from Ref. 4 for comparison, which also used an older material type. For more complete verification, additional specimens should be built and tested using fully characterized current materials, and complete data collected during the tests, including number of buckling waves, load-displacement curves, strain distributions, and failure modes. This would allow more detailed comparisons to be made with the FEA results, help identify and explain discrepancies, and would increase confidence in the methodology.

The PFA capability of MSC Nastran SOL 400 is a promising tool to predict final failure, rather than just initial failures, of laminated composite structures. It was shown in this paper that in certain cases, final global failure can occur at loads well above initial local failure (e.g. 8351 vs. 6046 lbs, Fig. 8). Therefore, SOL 400 PFA offers the potential to more fully utilize the capabilities of composite materials.

## Acknowledgements

Thanks to William Zivich, IRAD Principal Investigator for funding this study, John Scarcello (Manager) and Eric Horton (Senior Manager) for supporting attendance at the 2013 MSC Users Conference, and Hanson Chang and James Filon of MSC for providing sample input files and assistance in performing the analyses.

## References

1. Bulson, P.S., *The Stability of Flat Plates*, Elsevier, 1969
2. Gerard, G., *Handbook of Structural Stability, Part IV, Failure of Plates and Composite Elements*, Technical Note 3784, National Advisory Committee for Aeronautics, 1957
3. *Composite Materials Handbook, MIL-HDBK-17F, Volume 3, Polymer Matrix Composite Materials Usage Design and Analysis*, Department of Defense, 2002

4. Bonanni, D.L., Johnson, E.R., Starnes, J.H., “Local Crippling of Thin-Walled Graphite-Epoxy Stiffeners”, AIAA paper 88-2251, 1988
5. MSC Nastran 2012.2 *Quick Reference Guide*, Rev 0, June 26, 2012
6. Singer, J., Arbocz, J., Weller, T., *Buckling Experiments: Experimental Methods in Buckling of Thin-Walled Structures*, John Wiley & Sons, 1998